C. R. Mecanique 339 (2011) 362–368

Contents lists available at ScienceDirect

Comptes Rendus Mecanique

www.sciencedirect.com

Thermodiffusion and coupled phenomena / Thermodiffusion et phénomènes couplés

Digital interferometry as a powerful tool to study the thermodiffusion effect

Alexander Mialdun *, Valentina Shevtsova

Microgravity Research Center, Université Libre de Bruxelles, CP165/62, av. F. Roosevelt, 50, B-1050 Bruxelles, Belgium

ARTICLE INFO

Article history:
Available online 21 April 2011

Keywords:
Digital interferometry
Diffusion
Thermal diffusion
Soret cell
Soret effect

ABSTRACT

Interferometry is a trusted and widely used optical technique for measurements of the refractivity of objects, from which related quantities like temperature, or concentration can be determined. In particular, it is considered as most precise method for measuring diffusion in transparent fluids. A reason why this precise and powerful technique has not yet found application for measuring thermodiffusion obviously lies not in the accuracy of the method itself but rather in a set of some complementary factors. Consideration of the main factors affecting accuracy of thermodiffusion measurement by interferometry is one of topics of present work.

For the measurements of thermodiffusion by means of optical diagnostics, we use a classical Soret cell with transparent lateral walls clamped between two thermostabilized blocks. Although this system is generally stable with downward temperature gradient, some small lateral heat flux provokes residual convection which in turn disturbs the measurement. Ability of the method to locate and exclude from consideration the regions disturbed by convection is demonstrated for cells of different geometries. Cell design optimized with help of digital interferometry has been successfully used to measure Soret and diffusion coefficients in different binary mixtures.

1. Introduction

Throughout many decades interferometry has been actively used for the accurate measurement of diffusion coefficients in transparent solutions [1]. Attempts to apply it for measuring thermodiffusion date back to the 1950s (e.g. see [2]), but since then, the method did not get wide usage. One of reasons for that was the absence of a well-developed flexible interferogram processing technique. Moreover, the presence and deleterious effect of residual convection was already recognised at that time, but ways of cell optimization had a rather intuitive base then.

Nowadays computer-aided processing of digital fringe patterns is well established and widely used, providing interferometry with much more flexibility and power than in former times. In addition, the progress in computing pushed much development of design tools which are now widely available and easy to use. By combination of both tools (digital interferometry and thermal design based on numerical simulation) we have developed an optimized convectionless Soret cell and have established a procedure to measure the Soret and diffusion coefficients with good accuracy and reliability.

* Corresponding author.
E-mail addresses: amialdun@ulb.ac.be (A. Mialdun), vshev@ulb.ac.be (V. Shevtsova).

1631-0721/$ – see front matter
doi:10.1016/j.crme.2011.04.001

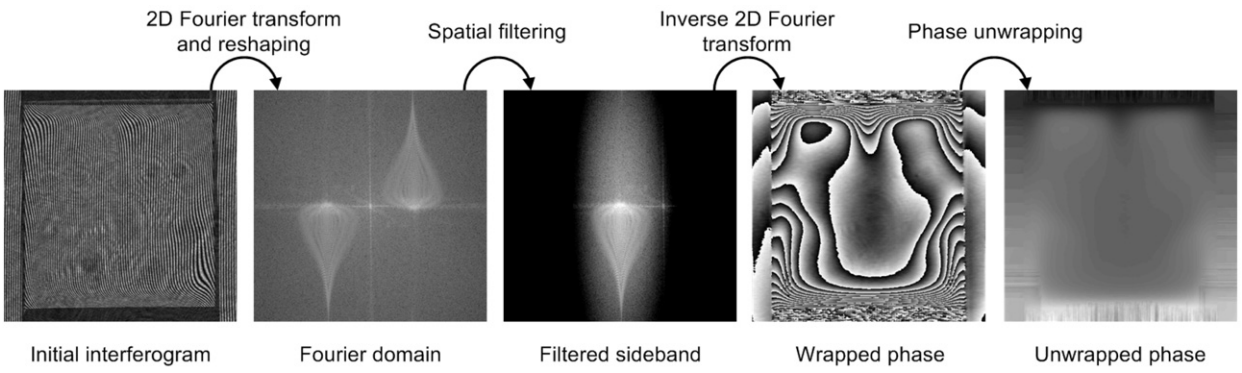

Fig. 1. Principle scheme of image processing steps.

2. Experiment and image processing

2.1. Experimental

For the measurements of the Soret effect by means of optical diagnostics, we have adopted a classical thermodiffusion cell with transparent lateral walls, open from the top and bottom and clamped between two thermostabilized copper blocks. We have tested two different cell geometries, one with an inner volume of $10 \times 10 \times 10$ mm^3, and another with $18 \times 18 \times 6.6$ mm^3. The glass frame of the cell is custom made of optical quality fused silica.

Each copper block is thermostabilized by a Peltier element driven independently by a PID controller enabling temperature stability of ± 0.01–0.02 K. Temperature logging is also provided by the controller with the resolution of 10^{-3} K. The data are recorded by computer with the desired sampling rate. The temperature gradient applied over cells was generally the same in all cases and close to 1 K/mm.

To observe the concentration variation inside liquid mixtures, the Mach–Zehnder interferometer scheme was applied since it allows simultaneous observation of the fringe pattern and the object itself and can easily treat the beam deflection problem. The light source is He–Ne laser with wavelength $\lambda = 632.8$ nm. The expanded and collimated laser beam is split into the reference and objective arms with the cell assembly placed within the last one. Then both beams are redirected by mirrors and join at the second beam splitter. The resulting interferogram is recorded by CCD camera. Resolution of imaging system is around 50 pixels/mm.

All optical components are mounted on optical bench plate, which is placed on top of the optical table but mechanically decoupled and thermally isolated from the latter. To improve the mechanical stability of interferometer, all elements were mounted on low rigid 25 mm diameter posts. To ensure the thermal stability of the interferometer during the experiment (up to 2–3 days), the whole setup including bearing bench plate is placed inside a box of thermal insulation material. The box is equipped with air-to-air cooling/heating assembly based on Peltier element and driven by the dedicated PID controller. A set of shields is inserted in the box to prevent air perturbation over optical paths. The temperature inside the box was kept equal to the mean temperature of liquid with residual fluctuations of ± 0.1 K.

Values of refractive index variation with temperature and concentration, $(\partial n/\partial T)_C$ and $(\partial n/\partial C)_T$ (the so-called contrast factors), are required for the measurement of species separation. When it was impossible to find these values in literature we had extracted them from a set of refractometric measurements.

We did experiments with two alcohol–water systems (namely, ethanol- and isopropanol-based) and with Fontainebleau benchmark [3] solutions (50/50 wt.% mixtures of dodecane (C12), isobutylbenzene (IBB) and 1,2,3,4-tetrahydronaphthalene (THN)).

2.2. Image processing technique

Presently there are two main methods available to extract spatial distribution of optical phase from interference patterns. They are: two-dimensional Fourier transform method [4,5] and temporal phase-stepping technique [6]. The latter one is considered as more sensitive, but former has an advantage to be more robust to external disturbances and needs only one snapshot to extract phase information. We have adopted the 2D Fourier transform method. As this method utilises the Fourier transformation of the fringe pattern, it places some requirements onto the latter. First, the carrier fringe system has to be sufficiently dense which will provide a distinguishable peak in the Fourier domain. At the same time, fringe contrast should not suffer when fringes are very close. More details one can find elsewhere [7]. Example of the fringe pattern with main processing steps is given in Fig. 1.

After 2D Fourier transformation of the initial fringe pattern one obtains a spectrum of fringes in the spatial frequency domain. A typical spectrum consists of three main features (see Fig. 1): a central peak with information about the background intensity of the interferogram, and two sidebands; each of them is carrying complete information about phase. One

needs to extract only one sideband from the full spectrum. For this purpose a Gaussian filter is applied to the spectrum with maximum located at the respective sideband.

The important step then is to shift the resulting spectrum towards the origin of Fourier domain. The distance of this shift corresponds to spatial frequency of initial (so-called reference) interference pattern (see Fig. 1). This operation removes the fringe carrier frequency from the spectrum and leaves only information about change of fringe density with respect to initial state, and value of phase related to this change. In addition to the fact that the reference interferogram determines the spatial carrier frequency, it possesses its own phase distribution map, which has to be evaluated in separate step and then to be subtracted from phase map of interest. In this way, the method applies the holography principle and tracks the only posterior optical phase variation in the set of images following the reference image.

By performing the inverse Fourier transform of the filtered and shifted spectrum, one can reconstruct both the amplitude and a spatial distribution of phase change of the fringe pattern. However, the phase difference calculated in this way is wrapped, which means that it belongs to the range $(-\pi, \pi)$, see Fig. 1. It should be unwrapped then to construct the continuous natural phase. Unlike the one-dimensional case, for two-dimensional and noisy maps, sophisticated unwrapping techniques are required. As in our case phase maps typically have a good quality, we adopt simplest approach based on successive comparison and validation of closed neighbour pixels. As a result, a smooth 2D phase map is obtained (see Fig. 1).

We had tested the interferometer stability and accuracy of reconstructed phase maps for standard experiment duration. Typical value of phase variation for interferometer working in thermostabilized box is $\pm 0.1 \ldots 0.2$ rad. The value agrees well with the common accuracy of interferometry ($2\pi/50$), which can be found in the literature [8].

In fact, the two-dimensional phase distribution (map) contains information about many things. The wave front can be distorted by optics, by perturbations of air temperature, by temperature distribution in glass walls, temperature distribution in liquid bulk, and finally by concentration distribution in the liquid. Each particular interference pattern is formed either by all above factors or by some of them, depending on the state of instrument. An important part of overall processing routine is the separation of contributions. This separation is done by choice of proper reference image. For example, by choosing reference image shortly after establishing the temperature difference over the cell, we can isolate information about all inputs into optical phase except concentration variation. Processing the next images with respect to this one provides the phase value, from which a full 2D map of concentration field is extracted by equation

$$C(x,z) = \left[\varphi(x,z) - \langle\varphi(x,z)\rangle\right] \frac{\lambda}{2\pi L} \Big/ \left(\frac{\partial n}{\partial C}\right)_T + C_0 \tag{1}$$

where $\varphi(x,z)$ is phase map extracted from specific fringe pattern, $\langle\varphi(x,z)\rangle$ is value of the phase averaged over field of view, L is optical path in liquid and C_0 is mean concentration of the mixture.

3. Cell optimization

The important aspects of the experiment, other than fringe processing, are the cell geometry and thermal design. This design is one of most critical factors, which can completely discard all advantages of interferometry. It determines presence and intensity of residual convection inside the cell. Due to drastically different characteristic times for transport of momentum and mass, the presence of convective flows in diffusion cell will significantly alter the concentration field. So, residual convection has to be reduced as much as possible.

When the thermal gradient is directed against gravity, the mechanical equilibrium in the cell is generally stable. However, convection can easily appear at lateral walls of the cell and in the corners where thermal perturbations are inevitable. For example, in our very first version of cubic cell it was impossible to see any thermodiffusion separation at all. Flow visualisation revealed presence of residual convection in this cell with velocity of 10–20 μm/s, which was enough to mask the concentration separation [9].

In view of the fact that similar problem of residual convection was addressed since very first measurements in classical Soret cell, we have started with stationary heat transfer calculations of the used and planned cell geometries. We utilised the Comsol Femlab package as it allows easy generation and treatment of complex geometries. For simulation, we took the thermal properties of copper, quartz glass, water, rubber and air from literature, and realistic boundary conditions.

First of all, we found a way of simple improvement of existing cell by replacing glass frame with thick walls by thin ones. Essential reduction of lateral temperature gradients was demonstrated both numerically and experimentally [10]. With such an improved cell it was possible to see a layer of liquid at central part where separation followed theoretical prediction (Fig. 2).

Although such a cell enables us to perform adequate measurements [9], disturbed regions in the cell corners were still very big. A next iteration of the cell, also inspired by numerics, was a flattened cell with larger optical path $L = 18$ mm and reduced height $H = 6.6$ mm. This new cell was bounded by completely flat copper blocks with no grooves or protrusions, which further reduced lateral heat fluxes. Sealing gaskets applied for this version of the cell were made of PTFE sheet of 0.2 mm thick. Although evidently reduced, lateral temperature gradients were still present in the cell. This in turn resulted in slight disturbance of concentration map in corners (Fig. 3).

With the same numerical tool we had finally found an ‘ideal’ solution for the cell which is completely free of heat fluxes through lateral walls. It is mainly based on previous cell geometry but with sealing gaskets made of material with thermal

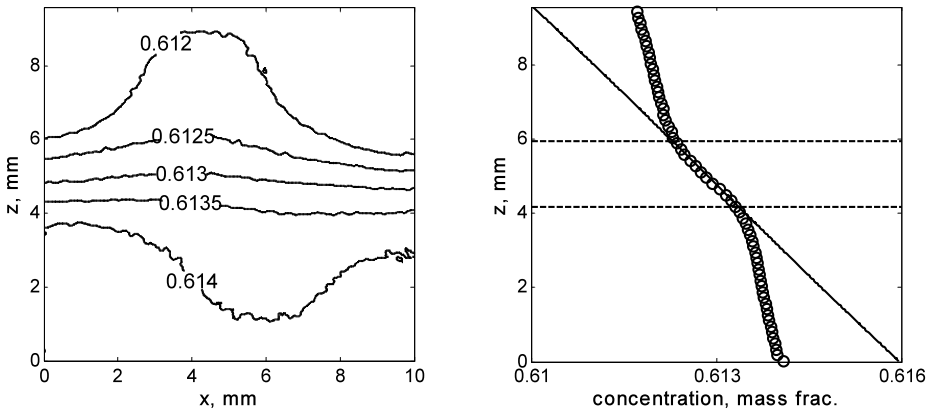

Fig. 2. Concentration map (left) and vertical profile at $x = 5$ mm (right) after separation of water–ethanol solution with 0.613 mass fraction of water in cubic cell. Open circles in right plot are experimental points, solid line is theoretical profile for given time instant and dashed lines confine central trustworthy layer.

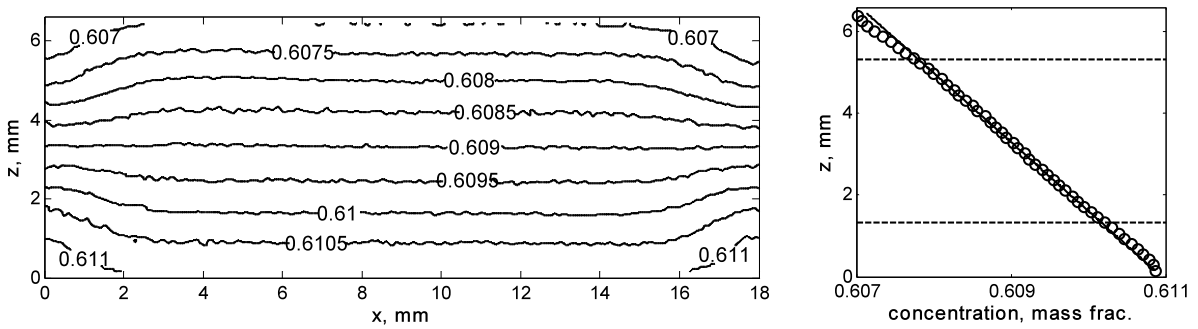

Fig. 3. Concentration map (left) and vertical profile at $x = 9$ mm (right) after separation of water–ethanol solution with 0.609 mass fraction of water in flat cell. Open circles in right plot are experimental points, solid line is theoretical profile for given time instant and dashed lines confine central undisturbed layer.

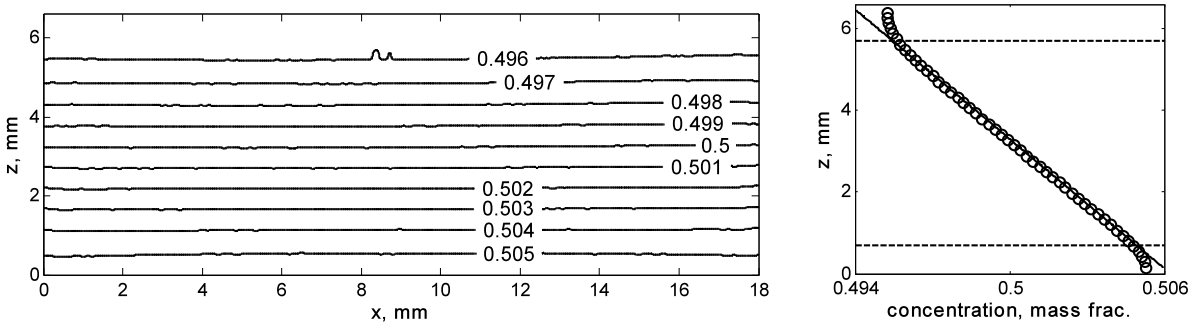

Fig. 4. Concentration map (left) and vertical profile at $x = 9$ mm (right) after separation of THN-C12 solution with 0.50 mass fraction of THN in flat cell with gaskets of special rubber. Open circles in right plot are experimental points, solid line is theoretical profile for given time instant and dashed lines confine central trustworthy layer.

conductivity equal to one of glass. Nowadays such materials are commercially available as thermal conductive composite rubber. In agreement with prediction, separation in such cell exhibits absence of disturbances at lateral walls (Fig. 4). Thus, iteratively we had approached the cell design suitable for precise measurements of Soret and diffusion coefficients.

4. Measurement of thermodiffusion and diffusion

The present technique gives a unique possibility of increasing measurement accuracy by providing information about concentration distribution all along the thermodiffusion path. In fact, the method gives a two-dimensional concentration map, although the distribution itself is almost one-dimensional. This excessive information can be used for evaluation of residual convection, but in the case when convection is really negligible, the 2D concentration map may be shrunk to a 1D

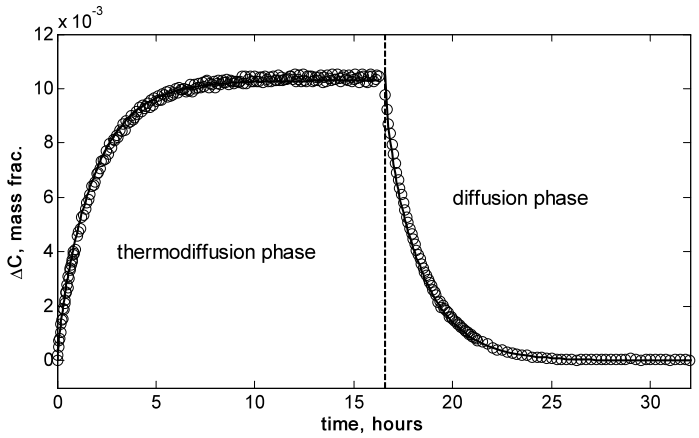

Fig. 5. Separation curves for THN-C12 solution with 0.50 mass fraction of THN. Open circles are experimentally measured concentration difference over field of view, solid lines are fitting curves.

concentration profile. So, at each time instant we have full concentration distribution over the thermodiffusion path. This extended dataset requires development of new procedure for extraction of coefficients.

The solution of thermodiffusion equations for convectionless case can be written as follows [9]:

$$C(z,t) = C_0 + C_0(1-C_0)S_T\Delta T\left[\frac{1}{2} - \frac{z}{L} - \frac{4}{\pi^2}\sum_{n,\text{odd}}\frac{1}{n^2}\cos\left(\frac{n\pi z}{H}\right)\exp\left(-n^2\frac{t}{\tau_r}\right)\right] \tag{2}$$

where S_T is Soret coefficient, ΔT is applied temperature difference, and $\tau_r = H^2/\pi^2 D$ is characteristic time, which determines the diffusion coefficient D.

The expected concentration is calculated for each experimentally observed point z_i and each time point of image acquisition t_i using two fitting parameters of S_T and τ_r with some initial guess for them. Then fitting is done iteratively by using the Nelder–Mead algorithm, which minimizes the misfit function:

$$\delta C = \sum_{i,j}^{k,m}\left[C_{\text{exper}}(z_i,t_j) - C_{\text{theor}}(z_i,t_j)\right]^2 \tag{3}$$

by varying the above fitting parameters. The number of spatial points in the experimental dataset is around $k = 340$ and the number of acquired images is $m = 200,\ldots,800$. So, the fitting is done with the matrix of at least $k \times m = 340 \times 200$ size. Due to such large amount of data, even this simple approach gives satisfactory results. However, the accuracy of fitting can be improved when possible sources of errors in the experimental data are considered and accounted for.

One of the errors, for example, comes from the fact that the reference image for extracting concentration distribution is not necessarily located at the very beginning of the separation step, as it has to be taken only after the temperature profile is completely established. Due to that, a reliable reference image can often be found in 5–10 minutes after the real separation start, although in the above fitting the time of reference image is $t = 0$ and $C_{\text{exper}}(z,0) = C_0$.

Correction for this error is rather evident and easy. One needs to introduce one more fitting parameter t_0, let us call it "initial time". Then the theoretical anticipation for experimental concentration profile is given by

$$C_{\text{theor}}(z,t) = C(z,t+t_0) - C(z,t_0) + C_0 \tag{4}$$

where both terms $C(z,t+t_0)$ and $C(z,t_0)$ are calculated according to (2). Such correction gives much better fit to spatial concentration profiles than simple use of Eq. (2).

An additional advantage of this experimental technique is the opportunity to track backward diffusion relaxation after switching off the temperature gradient over the cell. The linear concentration profile from which the diffusion relaxation starts from, allows easy derivation of solution describing the process:

$$C(z,t) = C_0 - \Delta C_{st}\left[\frac{4}{\pi^2}\sum_{n,\text{odd}}\frac{1}{n^2}\cos\left(\frac{n\pi z}{H}\right)\exp\left(-n^2\frac{t}{\tau_r}\right)\right] \tag{5}$$

where ΔC_{st} is separation after reaching steady-state, and τ_r is the only fitting parameter in this case. An example of experiment conducted in two steps is given in Fig. 5.

This measurement of coefficients in two steps allows further increase of accuracy, as the diffusion coefficient is measured twice. Then, the corrected diffusion coefficient can be introduced into equations for thermodiffusion to improve an accuracy of Soret coefficient fit.

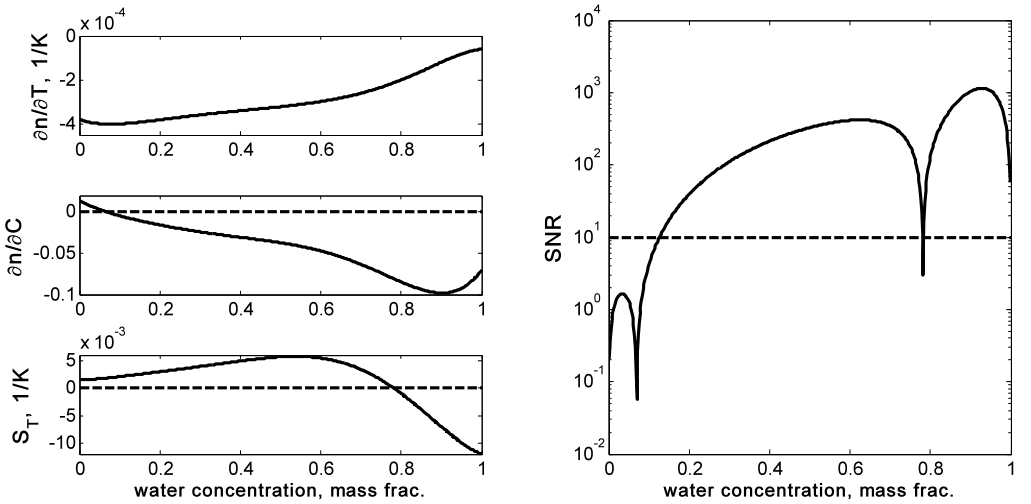

Fig. 6. Plots of concentration-dependant properties which determine signal-to-noise ratio (left). Signal-to-noise ratio over full concentration range for water–isopropanol system (right); dashed line is approximate threshold of reliable measurements.

Soret and diffusion coefficients of three Fontainebleau benchmark mixtures [3] have been measured by the above technique. Remarkably the values measured by digital interferometry agree with benchmark values within less than 3% [11].

Along with all advantages of the method there are some limitations as well. First, a negative Soret coefficient cannot be measured in such a high cell due to rapidly developing double diffusive instability. This problem can be avoided by use of a cell with thin liquid layer of millimetre height and inverse thermal gradient as it is usual in beam deflection method [12].

Another limitation of the method comes from the fact that it is based on optical diagnostics. It means that in some special cases accuracy of the method can go down due to certain optical and other properties of the mixture. A good exemplary system to consider such cases is a water–alcohol mixture. In all such systems every optical technique suffers from high scattering of data in range of small water concentrations. Particularly for the present method it means that separation curves (like those shown in Fig. 5) become very noisy in the region mentioned. The scattering of separation values follows from behaviour of observed vertical profiles which demonstrate strong oscillatory deviations from theoretical ones especially close to horizontal boundaries.

Reason for such data scattering is mixing in optical signal (phase) several inputs: main concentration input, optical noise and thermal noise. Of course, the basic temperature field is taken out of consideration by subtraction of respective reference image, but there are always some fluctuations of this field due to active thermal regulation. In many cases influence of these fluctuations is negligible, but when concentration input vanishes for some reasons, they become pronounced.

If we introduce a signal-to-noise ratio (SNR) which relates overall separation value to its fluctuations and transform it into ratio of measured quantities (phase), we can try to isolate main parameters influencing measurement accuracy:

$$SNR = \frac{\Delta C}{\delta(\Delta C)} = \frac{\Delta\varphi_C}{\delta(\Delta\varphi_C)} = \frac{\Delta\varphi_C}{\delta\varphi_T + \delta\varphi_{\text{opt}}} \tag{6}$$

If we skip in Eq. (6) the phase fluctuation $\delta\varphi_{\text{opt}}$ related to optical noise as it is typically order of magnitude less with respect to phase variation due to thermal noise $\delta\varphi_T$, we can obtain

$$SNR \approx S_T C_0(1 - C_0)\frac{(\partial n/\partial C)}{(\partial n/\partial T)}\frac{\Delta T}{\delta T} \tag{7}$$

where δT is temperature fluctuation value. So, finally the SNR depends upon three concentration-dependent quantities: both contrast factors and Soret coefficient. In Fig. 6 it is clearly seen how these quantities affect the SNR, namely, it has gaps in concentration points where any of these values vanishes.

At the point with zero S_T, the gap is very narrow since in this region the concentration input is large due to high $(\partial n/\partial C)$. Situation is much worse in region where contrast factor $(\partial n/\partial C)$ vanishes, separation itself is very small here due to small S_T and thermal noise is most pronounced due to highest $(\partial n/\partial T)$.

Presently, with current temperature stability, we can roughly estimate the threshold for reliable measurements by this method as $SNR = 10$, which is plotted in Fig. 6 by dashed line. There are some possibilities to decrease the threshold by improvement of thermal regulation system and/or by studying spatial behaviour of temperature fluctuations.

5. Conclusion

Modern developments in digital imaging and image processing have drastically improved flexibility and usability of interferometry for measurement of transport properties of transparent fluids.

In addition to pure diffusive convectionless measurements, convective instabilities can be easily recognised and localised by the technique allowing detection and elimination of problems coming from improper cell design.

Diffusion and thermodiffusion coefficients can be reliably and accurately measured in single- or two-step experiments.

A way of estimating the applicability range of the method is presented.

Acknowledgements

The authors are grateful to Prof. J.C. Legros and Prof. F. Dubois for valuable discussions. This work was supported by the PRODEX programme of the Belgian Federal Science Policy Office and European Space Agency.

References

[1] C. Tropea, A. Yarin, J. Foss (Eds.), Springer Handbook of Experimental Fluid Mechanics, Springer-Verlag, Berlin, Heidelberg, 2007.
[2] L.G. Longsworth, The temperature dependence of the Soret coefficient of aqueous potassium chloride, J. Phys. Chem. 61 (1957) 1557–1562.
[3] J.K. Platten, M.M. Bou-Ali, P. Costeseque, et al., Benchmark values for the Soret, thermal diffusion and diffusion coefficients of three binary organic liquid mixtures, Philos. Mag. 83 (2003) 1965–1971.
[4] M. Takeda, H. Ina, K. Kobayashi, Fourier-transform method of fringe-pattern analysis for computer-based topography and interferometry, J. Opt. Soc. Amer. 72 (1982) 156–160.
[5] W.W. Macy Jr., Two-dimensional fringe-pattern analysis, Appl. Opt. 22 (1983) 3898–3901.
[6] K. Creath, Phase-measurement interferometry techniques, in: E. Wolf (Ed.), Progress in Optics, vol. XXVI, Elsevier Science Publishers, 1988.
[7] D. Malacara, M. Servin, Z. Malacara, Interferogram Analysis for Optical Testing, 2nd ed., Taylor & Francis, 2005.
[8] M. Hipp, J. Woisetschläger, P. Reiterer, T. Neger, Digital evaluation of interferograms, Measurement 36 (2004) 53–66.
[9] A. Mialdun, V. Shevtsova, Development of optical digital interferometry technique for measurement of thermodiffusion coefficients, Int. J. Heat Mass Transfer 51 (2008) 3164–3178.
[10] A. Mialdun, V. Shevtsova, Open questions on reliable measurements of Soret coefficients, Micrograv. Sci. Technol. 21 (2009) 31–36.
[11] A. Mialdun, V. Shevtsova, Measurement of the Soret and diffusion coefficients for benchmark binary mixtures by means of digital interferometry, J. Chem. Phys. 134 (2011) 044524.
[12] A. Königer, B. Meier, W. Köhler, Measurement of the Soret, diffusion, and thermal diffusion coefficients of three binary organic benchmark mixtures and of ethanol–water mixtures using a beam deflection technique, Philos. Mag. 89 (2009) 907–923.